



Dissolutive flow in nanochannels: transition between plug-like and Poiseuille-like

Qing Miao^{1,2} · Quanzi Yuan^{1,2} · Ya-Pu Zhao^{1,2}

Received: 6 July 2018 / Accepted: 9 October 2018 / Published online: 21 November 2018
© Springer-Verlag GmbH Germany, part of Springer Nature 2018

Abstract

Dynamic properties of dissolutive flow in nanochannels were investigated by molecular dynamics simulations. It turned out that the liquid flow pattern changes greatly after the dissolution effect taken into consideration. Liquid inside the channel has a plug-like velocity profile when the dissolubility is low, whereas a Poiseuille-like flow was observed as the dissolubility increases. By introducing the dissolution term to molecular kinetic theory, we explained the physical mechanisms of velocity transition. During which a modified dimensionless Galilei number was proposed to describe the effect of main forces. The results showed that in pressure-driven flow, when the dissolubility is low, the dominant dissipation is the viscous dissipation and the theoretical model of insolubility is acceptable. However, as the dissolubility increases, the dissolving dissipation takes priority, which results in the velocity profiles becoming Poiseuille-like. In addition, we analyzed the evolution of fluid density, number of dissolved solid particles and concentration distribution of solute. The liquid density varying from layered oscillation to uniform distribution was obtained, which can be described by a critical number. The analysis of solute concentration helps to establish the scaling relation among the dissolution rate, convection velocity, and diffusion coefficient. These findings not only help to understand the physical mechanisms of dissolutive flow but also help to control and optimize the flow patterns in dissoluble channels.

Keywords Dissolutive flow · Nanochannels · Transport properties · Molecular dynamics simulation

This article is part of the topical collection “2018 International Conference of Microfluidics, Nanofluidics and Lab-on-a-Chip, Beijing, China” guest edited by Guoqing Hu, Ting Si and Zhaomiao Liu.

Electronic supplementary material The online version of this article (<https://doi.org/10.1007/s10404-018-2146-1>) contains supplementary material, which is available to authorized users.

✉ Quanzi Yuan
yuanquanzi@lnm.imech.ac.cn

✉ Ya-Pu Zhao
yzhao@imech.ac.cn

¹ State Key Laboratory of Nonlinear Mechanics, Institute of Mechanics, Chinese Academy of Sciences, Beijing 100190, People’s Republic of China

² School of Engineering Science, University of Chinese Academy of Sciences, Beijing 100049, People’s Republic of China

1 Introduction

Dissolutive flow occurs when liquid flows over and simultaneously dissolves its solid surface. Due to its importance in both practical applications and academic research, the dissolutive flow has received considerable attention. It plays a significant role in energy (Poesio et al. 2009), metal ablation (Ivanisenko et al. 2003; Marzun et al. 2017), drug dissolution (Amidon et al. 1995), and other fields (Daccord and Lenormand 1987). For instance, the formation of salt cavities mainly adopts the way of water-soluble mining (Anderson and Kirkland 1980), during which the precise control of dissolution is of great significance. Over the last few decades, much of excellent work has considered the fluid flow on non-dissoluble substrates (Bonn et al. 2009; Brutin and Starov 2018; De Gennes 1985; Fan et al. 2002). It was found that the no-slip boundary condition is not always applicable to microscopic flow. Navier introduced a well-known linear slip boundary model ($b \sim u_x/\dot{\gamma}$) (Navier 1823). Subsequently, the kinetic slip model was proposed by Pismen and Rubinstein (2001). Lichter et al. presented the variable

density Frenkel–Kontorova model (vdFK model) which revealed that slip occurs at the solid surface via two mechanisms (Lichter et al. 2004; Martini et al. 2008). In these inert flows, a plug-like flow in nanochannel was observed, as depicted in Fig. 1c. Compared with the classical Poiseuille flow in parallel plate, it has been found that the effect of the channel size (Netos et al. 2005; Lichter et al. 2004; Sofos et al. 2009), properties of the substrate (Nagayama and Cheng 2004; Sofos et al. 2010, 2011), as well as the competition of the driving force and resistance (Martini et al. 2008; Wang and Zhao 2011) play a significant rule in the transition from Poiseuille-like to plug-like flow. However, there is still a lack of an explicit analysis when the dissolution effect is included. Besides, plenty of density properties during inert flow were analyzed (Alexiadis and Kassinos 2008; Thomas and McGaughey 2008). Granick once proposed that the confined fluid demonstrates the tendency of variable density (Granick 1999), as shown in Fig. 1d. When the dissolving factor is taken into consideration, the flow pattern will be more complex due to the coupling transport of mass and momentum. As described in Fig. 1e–h, the velocity profile is not plug-like but Poiseuille-like, the density distribution tends to be uniform but not fluctuant. This means that we can regulate the characteristics of fluid in dissolvable channels by controlling the dissolubility of solid in liquid. The inert flow theories are no longer applicable to applications involving dissolution, which requires us to explore the physical mechanisms behind dissolution behaviors.

Previously, dramatic breakthroughs of dissolution behaviors have been made in metal/metal (Benhassine et al. 2011; Odzak et al. 2014; Yin et al. 2006), metal/ceramic (Landry and Eustathopoulos 1996; Zhou and De Hosson 1996), metal/acid (Bentiss et al. 2005) systems. Nevertheless, the optical opacity of metal and ceramic material raises great challenges to track the evolution of the solid/liquid boundary, and the requirement of anti-oxidation greatly limits the experimental operation (Singler et al. 2012). Additionally, pioneering work has been done on drug dissolution (Siepmann and Siepmann 2013), droplet dissolution of the transparent substrates (Yang et al. 2018), and the dissolution behaviors in porous media (Bekri et al. 1995; Daccord 1987) that analyzed the fractal patterns and fractal dimension. However, the physical mechanisms of dissolutive flow in channels are still far from well understood.

In this paper, we studied the characteristics of confined fluid and dissolved solid particles by utilizing molecular dynamics (MD) simulations. Fluid velocity transition between plug-like and Poiseuille-like was observed. While the effect of competition between the dissolving and viscous dissipation was analyzed. Further, the concentration distribution of dissolved particles was obtained. We concluded that the dissolution behavior in nanochannels can be controlled by changing the dissolubility of solid in liquid. These findings can help us understand more about the physical mechanisms of dissolutive flow and we hope to set a theoretical foundation for its applications.

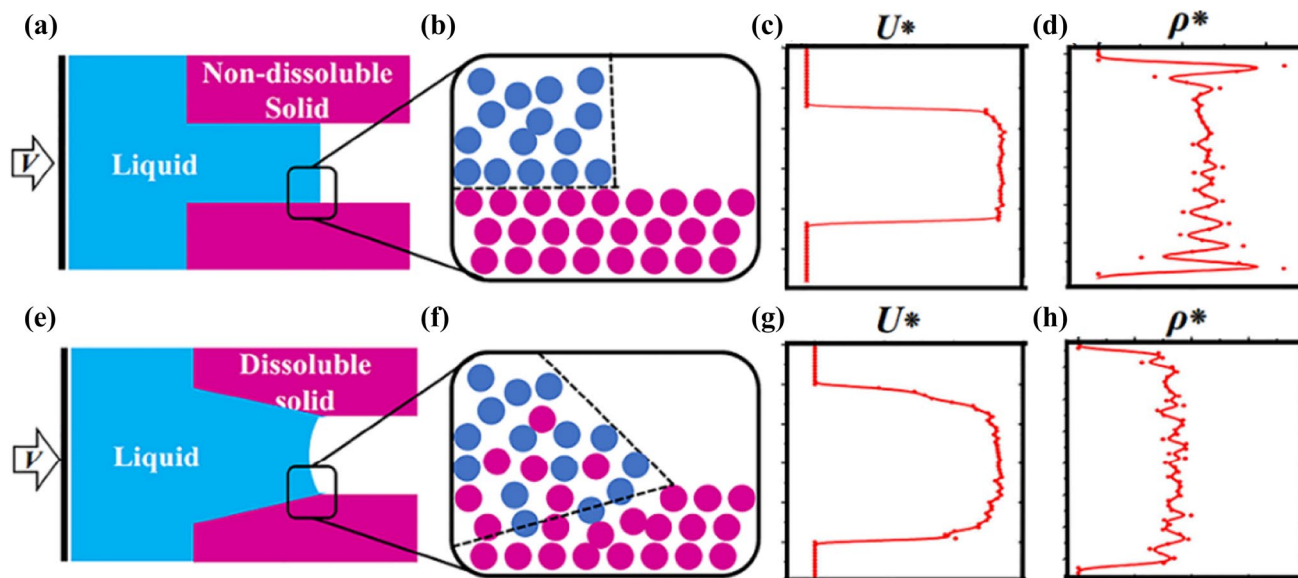


Fig. 1 Schematics of **a** liquid flows through a non-dissolvable nanochannel, **b** molecular structure of non-dissolvable solid–liquid interface, **c** plug-like velocity profile, **d** liquid density that presents an oscillating distribution, **e** liquid flows through a dissolvable nanochan-

nel, **f** molecular structure of dissolvable solid–liquid interface, **g** Poiseuille-like velocity profile, and **h** the liquid density that is uniform in nanochannel. (Color figure online)

2 Molecular dynamics simulations

LAMMPS (Plimpton 1995) is used to simulate the dynamic behaviors of fluid in nanochannels. As depicted in Fig. 2a, our model consists of three parts. The liquid in blue is explored as extended single point charge (SPC/E) water model. The density, viscosity, and surface tension of water are set as $\rho = 994 \text{ kg/m}^3$, $\mu = 0.729 \text{ mPa s}$, and $\gamma = 0.0636 \text{ N/m}$, which are close to experimental values at 300 K and 1 bar (Berendsen et al. 1987). Atoms in pink are the dissolvable solid atoms. Atoms in gray are non-dissolvable which provide the impetus for the movement of water molecules with a constant speed $V_0 = 1 \text{ m/s}$. Loading forces by controlling displacement is widely used to study the flow in nanochannels driven by pressure (Chen et al. 2008; Joseph and Aluru 2008). Figure 2b shows the overall process of MD simulations.

The interaction between molecules is mainly determined by two parts as many recent investigations (Grujicic et al. 2004; Werder et al. 2001):

$$E_{ij} = 4\epsilon_{ij} \left[\left(\frac{\sigma_{ij}}{r_{ij}} \right)^{12} - \left(\frac{\sigma_{ij}}{r_{ij}} \right)^6 \right] + q_i q_j / \epsilon_0 r_{ij}. \quad (1)$$

The first part is the Van der Waals interaction (VDW) that can be described by Lennard-Jones (LJ) potential (Lennard-Jones 1931). In which ϵ_{ij} , σ_{ij} , and r_{ij} indicate the depth of the potential well, the effective molecular diameter, and the distance between two atoms i and j ,

respectively. The second part is the Coulomb potential, where ϵ_0 is the electrostatic constant. The oxygen atoms and hydrogen atoms are charged LJ particles with $q_O = -0.8476 \text{ e}$, and $q_H = +0.4238 \text{ e}$, respectively. This interaction is also used to calculate the critical state during dissolution which will be shown in detail later. A cutoff radius of 1 nm is used. The time step is set to be 1 fs. All simulations are run in NVT ensemble under periodic boundary conditions. Nosé–Hoover thermostats are used to maintain the liquid temperature at 300 K. Simulations varying among different channel widths and dissolubility are discussed, including $d/D = 0.24, 0.30, 0.37, \epsilon = 0.65, 0.81, 0.97$, and 9.71 , where d, D , and $\epsilon = \epsilon_{s-s} / \epsilon_{s-l}$ represent the channel width, the total length in the y direction, the ratio of solid–solid and solid–liquid interactions, respectively. The smaller the ϵ is, the higher the dissolubility is. As for the simulation parameters, the exact values of the interaction between particles as well as the channel widths are given in supplementary material (Tables S1, S2). The solid–liquid interaction is fixed so that the wettability is unchanged. A hydrophilic solid–liquid interaction is selected and the corresponding contact angle is nearly 50° . Besides, the dissolvable interaction of solid particles is similar to the dissolution of ionic crystals. By changing the solid–solid interactions, we change the dissolubility. When $\epsilon = 9.71$, it means that the solid particles cannot be dissolved and this simulation is carried out to compare our results with the non-dissolvable situation.

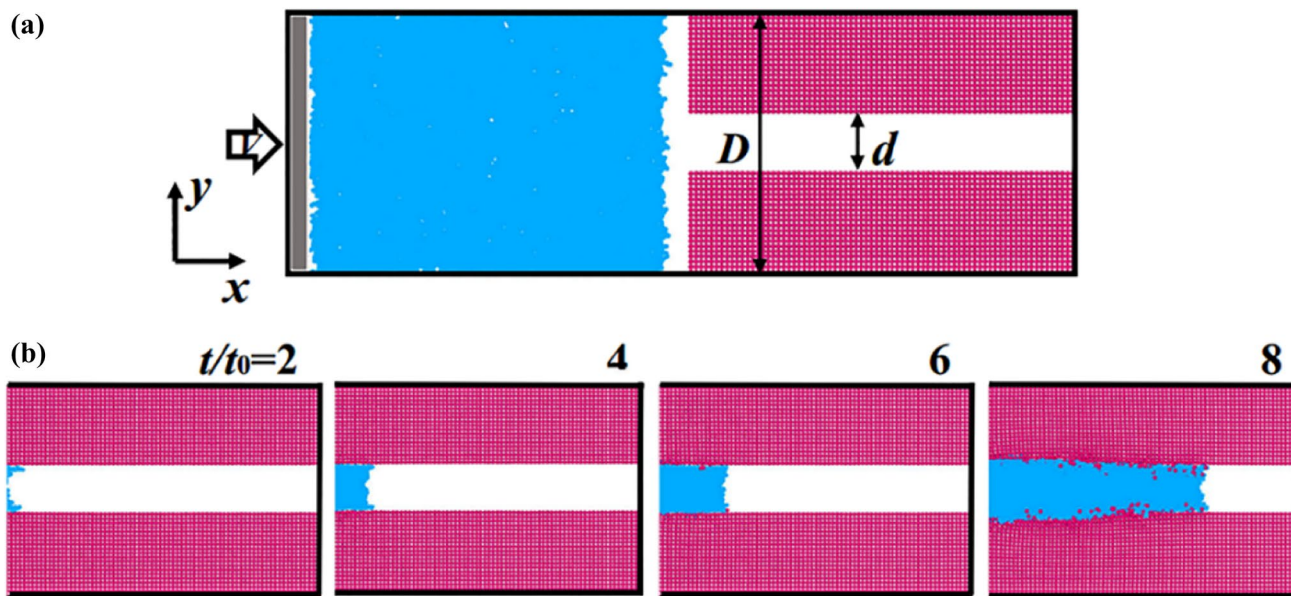


Fig. 2 a The simulation domain is composed of three parts: solid surface atoms (pink), water molecules (blue), and wall atoms (gray) that push the water into the channel. b Evolution of dissolutive flow: liquid dissolves the solid particles while it flows through the nanochan-

nel and the numbers in upper right corner indicate the dimensionless time d and D , respectively, represent the channel width and the whole width of the model in the y direction. (Color figure online)

3 Results and discussion

3.1 Velocity transition between plug-like and Poiseuille-like

Figure 3 depicts the dimensionless velocity profiles along the x direction. Due to the similarity of velocities in different cross sections (see in the Supplementary Material), a specific section is selected to calculate the velocity profiles. It is obvious that as channel width increases, the fluid velocity in a section within the channel decreases, which is consistent with the dynamics of macroscopic fluid flow that can be explained by continuity equations. Besides, the transition between plug-like and Poiseuille-like flow occurs with the variation in dissolving capacity. The physical mechanisms of this transition were explored through multiscale theory combined with molecular kinetic theory (MKT) and fluid mechanics. By introducing MKT (Laidler et al. 1941; Wang and Zhao 2011), we know that the fluid flow on solid surface can be treated as a rate process. Liquid particles need to overcome the potential energy barrier E_0 when they randomly walk between the adjacent adsorption sites separated by a distance λ . In the equilibrium state, the liquid particles jump forward and backward in the same frequency. When the system is affected by external forces, the frequency can be amended as:

$$\kappa = k_B T F_+ / h F_0 \exp[(\omega/2 - E_0) / k_B T] - k_B T F_- / h F_0 \exp[(-\omega/2 - E_0) / k_B T], \tag{2}$$

where h , k_B , T , $\omega/2$, F_+ , and F_0 represent the Planck constant, the Boltzmann constant, the absolute temperature, the change in energy barrier, the partition function of activated and initial state, respectively. When the external forces work, the energy barrier changes. The liquid molecules are

more likely to move forward, and their backward frequency decreases. Thus, the liquid flows in a particular direction and the net frequency κ of liquid directional movement is obtained. And ω can be expressed as:

$$\omega = -G \sin \theta_2 - \tau_x \lambda^3 + p_x \lambda^2 h + (\gamma_{LVf} \cos \theta_{1f} - \gamma_{LV} \cos \theta_1) + (\gamma_{SLf} \cos \theta_{2f} - \gamma_{SL} \cos \theta_2), \tag{3}$$

in which G , θ_2 , θ_1 , τ_x , p_x , h , γ_{LV} , and γ_{SL} represent the dissolving energy, angle between the liquid that dissolves into the solid and the horizontal wall surface, angle between the upper liquid and the horizontal wall surface, shear stress, pressure, characteristic length in the vertical direction, the liquid–gas and the solid–liquid interfacial energy, respectively. In our simulations, the dissolving resistance $-G \sin \theta_2$, viscous resistance $-\tau_x \lambda^3$, and driving energy $-p_x \lambda^2 h$ that caused by the pressure, are all considered. The changes of the surface energy $(\gamma_{LVf} \cos \theta_{1f} - \gamma_{LV} \cos \theta_1) + (\gamma_{SLf} \cos \theta_{2f} - \gamma_{SL} \cos \theta_2)$, that caused by the changes of the surface tension here, is at least one order of magnitude smaller than other factors (as shown in the Supplementary Material) and can be neglect. Obviously, the driving force is caused by the pressure, and the resistance is the viscous and dissolving force. Here, we propose a modified dimensionless Galilei number to qualify the effect of these forces:

$$Ga' = \Delta F / [\mu^2 (1 + 1/Sc^2) / \rho], \tag{4}$$

in which ΔF and Sc are driving force and the Schmidt number, respectively. The Schmidt number: $Sc = \mu / \rho D_1$, represents the ratio of momentum and mass diffusivity, here D_1 is the diffusion coefficient. Provided that the dissolubility is low and negligible, the Sc is big and Ga' will converge to $Ga = \Delta F / (\mu^2 / \rho)$, (Wang and Zhao 2011). In this case, the main resistance is the viscous force μ^2/ρ , but it is pretty small in nanochannels. As a result, the flow tends to be plug-like as

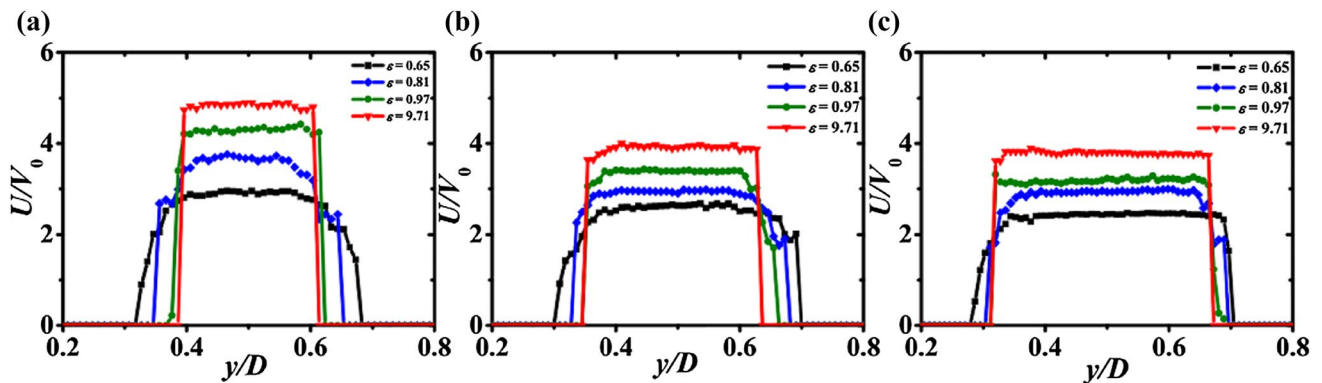


Fig. 3 Dimensionless velocity profile changes with respect to different channel widths and dissolubility, in which $V_0=1$ m/s is the wall velocity. **a** $d/D=0.24$, **b** $d/D=0.30$, and **c** $d/D=0.37$ represent different channel widths. The redlines with triangles, olive lines with pots,

blue line with rhombus, and black lines with squares represent different dissolubility of $\epsilon=9.71, 0.97, 0.81$, and 0.65 , where $\epsilon = \epsilon_{s-s} / \epsilon_{s-l}$ represents the ratio of solid–solid to solid–liquid interaction. The smaller the ϵ is, the higher the dissolubility is. (Color figure online)

most MD simulations (Chen et al. 2008; Hanasaki and Nakatani 2006). But with the increase in dissolubility ($\epsilon=0.65$ or $\epsilon=0.81$), the Sc becomes smaller, and the dissolving resistance $\mu^2 l \rho / Sc^2$ becomes more apparent and the fluid is no longer layered. Accordingly, the velocity distribution tends to be Poiseuille-like.

Moreover, solid–liquid boundary is important in nanoscale. As the solute particles dissolved, the solid wall become rougher and will affect the liquid behavior in nanochannels. Kasiteropoulou et al. found that the liquid velocities in nanochannels decreases as the effect of wall protrusion considered. Kasiteropoulou et al. (2013), which is consistent with our simulation results. Liakopoulos et al. described the effect of boundary on liquid at nanoscale by analyzing the Darcy–Weisbach friction factor where it was found that wall slip conditions, viscosity and transport properties are different in nanoscale and traditional continuum theory due to the nature of nanochannels (Liakopoulos et al. 2017). Thus, so as to characterize the liquid velocity near the solid surface, the slip length is calculated by definition: $b = u / \dot{\gamma}$. Slip length is a very important physical quantity to characterize fluid behavior and is strongly influenced by many factors, such as surface wettability (Ramosalvarado et al. 2016), wall roughness (Sofos et al. 2010, 2011) and interfacial nanobubbles (Yen 2015). Nevertheless, the effect of dissolution on the slip length is not clear. So, the slip length under different dissolubility and different channel widths are calculated. All slip lengths obtained are listed in Table 1.

Taking $d/D=0.24$ as an example, we depicted the slip lengths and velocity profiles in Fig. 4. It can be seen that in the case of high dissolution, the parabola fitting between the two vertical lines connects perfectly with the straight-line fitting outside the two vertical lines. Nevertheless, there is a significant turning point between the parabola fitting and the straight-line fitting in the case of low dissolution. Besides, the slip lengths of the Poiseuille-like flow are close to that of the plug-like flow. All of these indicate that the velocity distribution in the dissoluble channel is no longer plug-like but Poiseuille-like. This further confirms that the transition between the viscous and dissolving dissipation leads to the change of flow patterns in nanochannels. We can control the dynamics of dissolutive flow by altering the dissolubility of solid in liquid. To understand more about the effect of dissolution, we identify the density of liquid and properties of dissolved solid particles in following parts.

Table 1 Slip length b (Å) under different conditions

	$\epsilon=0.65$	$\epsilon=0.81$	$\epsilon=0.97$	$\epsilon=9.71$
$d/D=0.24$	12.50	17.70	34.95	36.32
$d/D=0.30$	9.99	15.13	31.97	35.60
$d/D=0.37$	6.56	10.82	28.92	31.17

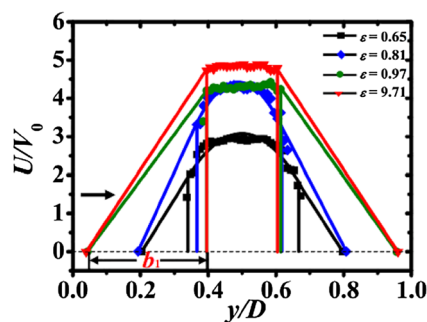


Fig. 4 The slip lengths and velocity profiles with different dissolubility, including $\epsilon=0.65, 0.81, 0.97,$ and 9.71 . The red triangles, olive pots, blue rhombus, and dark rectangles represent the velocity profiles. The smooth lines between and outside the two vertical lines are the parabola and line fitting of the velocity profile, respectively. The slip length b is obtained by definition. (Color figure online)

3.2 Density distribution

Density distributions of the fluid in nanochannels are calculated. When fluid flows through solid substrates, the solute molecules diffuse into liquid. As a consequence, the shape of the solid–liquid interface changes over time, therefore it is inappropriate to calculate density distribution by directly dividing the simulation region in the y direction into several layers like that in inert flow processes (Bakli and Chakraborty 2013). The simulation domain should also be divided in the x direction and then Lagrange interpolation method is used to modify the results. As shown in Fig. 5, when the dissolubility is low ($\epsilon=0.97$), the density of fluid presents an oscillating distribution and there is a peak near the solid wall, which is very close to the density distribution of non-dissoluble situation ($\epsilon=9.71$). This is because that in nanoscale, if the dissolubility is subtle, the confined liquids are mainly influenced by solid surfaces, then the layered phenomenon which results in the density oscillation occurs. However, with the increase of dissolubility ($\epsilon=0.65$), the oscillation characteristic of the density distribution disappears. Since dissolved solute alters the intrinsic nature of the confined liquids, making their molecular arrangement more disordered, and the layered structure is disrupted. Moreover, the variation of the peak value with dissolubility is shown in Supplementary Materials (Fig. S4) to illustrate the changes of the liquid atomic configuration. The density distribution here can be expressed as:

$$\rho(r) = \rho_0 \exp [(-w + G) / k_B T], \tag{5}$$

where G is the dissolution energy that inhibits the occurrence of the density layering and w is the disjoining pressure (Derjaguin and Obuchov 1936). We can see that the density of water near the wall decreases with the increases in dissolubility, this is in that the dissolved atoms occupying the positions of original water molecules and generating

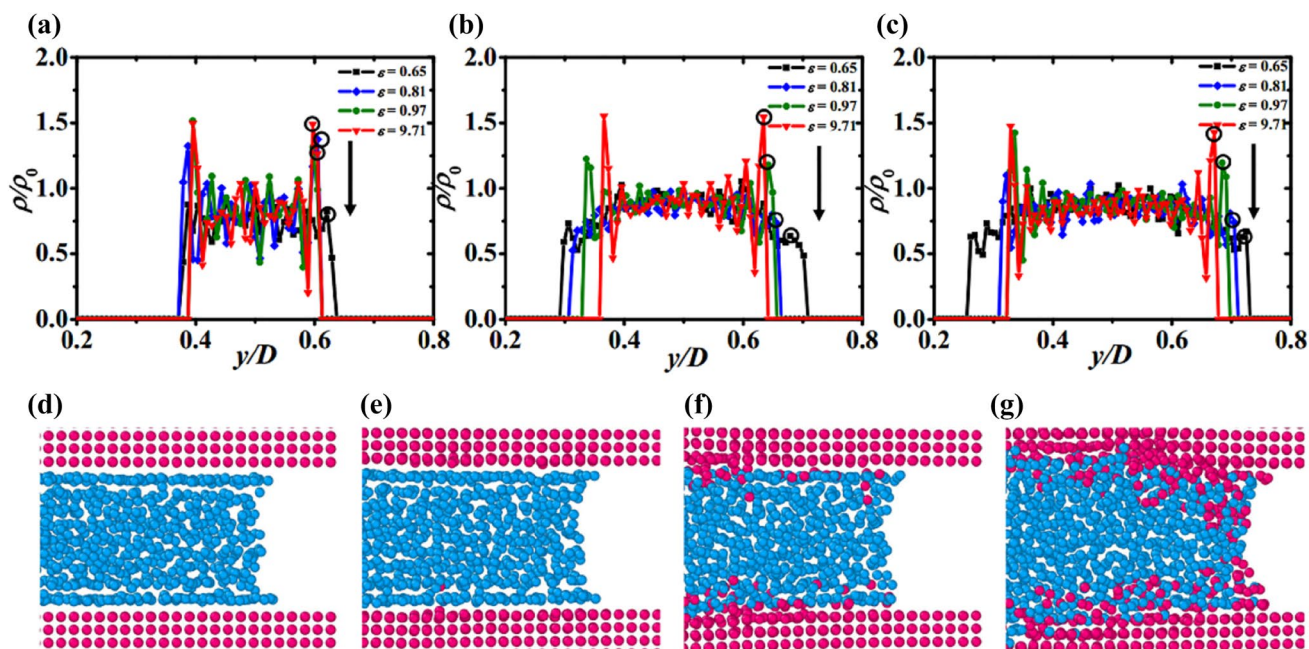


Fig. 5 Evolution of density distribution among different channel widths and dissolubility. **a** $d/D=0.24$, **b** $d/D=0.30$, and **c** $d/D=0.37$ show the density distributions under different channel widths. **d–g**

illustrates the liquid structure from our MD simulations with different dissolubility, including $\varepsilon=9.71$, 0.97, 0.81, and 0.65. (Color figure online)

disturbances to the orderly arranged liquid molecules near the solid walls. With the enhanced dissolution of solid in liquid, the disturbances rise and destroy the solid-like structure of liquid. This process increases energy dissipation near the wall, so the velocity profile becomes Poiseuille-like. Besides, the effect of dissolved atoms on the density variation, as well as the radial distribution function of liquid molecules nearby the surface has also been calculated in supplementary material (Figs. S5, S6). We found that the liquid near the solid wall is solid-like and the density transition always occurs whether the dissolved atoms are counted or not, the arrangement of the fluid molecules becomes more disorder with the dissolubility increases.

The most interesting thing is that when $\varepsilon=0.81$, the density of liquid near the surface is almost equal to that in the center of the channel. The density distribution realizes the transition from fluctuant state to uniform state. Thus, we can assume that ε exists a critical state ε_c , under ε_c the dissolution dominates the density structure, while above ε_c the size effect which results in the density fluctuation is more important. The critical value of ε_c that equals to 0.88 is obtained and analyzed in detail in Supplementary Material.

3.3 Dissolved particles and scaling analysis

As mentioned above, when fluid flows through the nanochannels, the dissolved solid particles alter the characteristics of solid–liquid interface and affect the internal

properties of liquid. Therefore, the number of dissolved solid particles is analyzed over time. As depicted in Fig. 6, the black squares, red dots and blue triangles are the results of $\varepsilon=0.65$, 0.81, and 0.97, respectively. While the red lines in all three pictures represent Boltzmann fitting curves. Obviously, the number of dissolved particles satisfies Boltzmann distribution pretty well:

$$N_{KV} = (N_1 - N_2) / [1 + e^{(t-t_0)/\Delta t}] + N_2, \quad (6)$$

here, N_{KV} , t_0 , N_1 , and N_2 , represent the number of dissolved particles at time t , the time at which the number of dissolved particles reaching half of the total dissolved number, the number of initial and final dissolved particles, respectively. During this process, the variation of the density profiles and the slip lengths are also calculated in Supplementary Material (in Fig. S3). Furthermore, by analyzing the different dimensionless ε values, we can find that the ratio of solid–solid and solid–liquid interaction has a profound effect on dissolution: when the ratio is equal to 0.97, the dissolubility is very low, and it almost has no effect on the liquid properties; when the ratio is between 0.81 and 0.65, the number of dissolved particles increases significantly and this will have a great disturbance to the nature of liquid. Through statistics of the number of dissolved particles can describe the degree of dissolution. From Fig. 6, we can see clearly that as the convection velocity increases, the number of dissolved particles is easier to reach a stable state. In other words, the

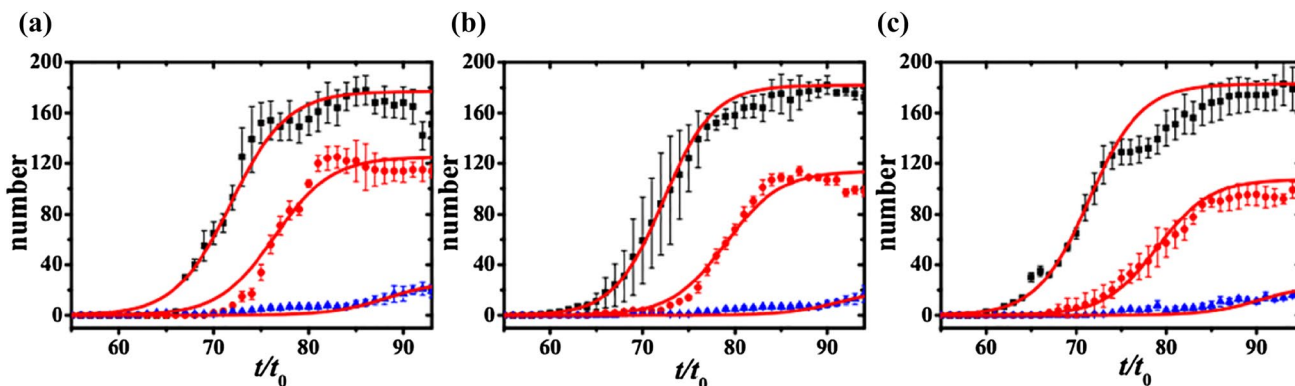


Fig. 6 Numbers of dissolved solid particles among different channel widths and dissolubility are analyzed over time. **a** $d/D=0.24$, **b** $d/D=0.30$, and **c** $d/D=0.37$. The black rectangle is the result of $\epsilon=0.65$, the red dots represent the outcomes of $\epsilon=0.81$, and the blue

triangles show the consequences of $\epsilon=0.97$, while the red lines in all three pictures represent the Boltzmann distribution fitting curves. (Color figure online)

dissolution is not only influenced by the dissolubility of solid in liquid but also affected by the convection velocity along the nanochannels.

On this basis, we analyzed the dissolution velocity of solute when the number of dissolved particles reached a steady state. The dissolution rate of a section was measured over time under different channel widths and dissolubility, and the statistic results are shown in Fig. 7. It is obvious that there exists a concentration boundary similar to macroscopic study (Schlichting and Gersten 2017) if the dissolving capacity is high ($\epsilon=0.81$ or $\epsilon=0.65$). In these two cases, the scaling analysis was carried out. The Nernst–Brunner equation is used to specify our model (Dokoumetzidis and Macheras 2006):

$$dm/dt = A \times D_1 \times (C_s - C) / \delta_c, \tag{7}$$

where dm/dt , A , δ_c , C_s , and C are the quality of dissolution per unit time, the solid–liquid contact area, the thickness of the concentration boundary, the saturation concentration, and the concentration of the solute at statistical moment, respectively. There are several hypotheses here: the contact area in the x direction is proportional to convection velocity U and a fixed section is analyzed; the solute concentration near the wall is C_s and the solute concentration in the bulk liquid is zero. Under these circumstances, Eq. (7) can be verified in our simulation, and the detailed information are given in Supplementary Material. Afterward, it can be seen that the dissolution rate v is inversely proportional to the thickness of the concentration boundary layer δ_c , which is consistent with the work of the Leif Ristroph in macroscopic dissolution behavior (Huang et al. 2015). In addition, there is a momentum boundary layer δ_m near the wall and the ratio of the two boundaries is also the Schmidt number Sc , in which $\delta_m \sim \sqrt{\mu x / \rho U}$ is obtained from the Prandtl boundary-layer equation and x is the characteristic length. Based on this, the

relation between diffusion coefficient and dissolution rate indicates:

$$v\sqrt{xv} / \sqrt{U} \sim D_1 \sim f(\epsilon, d/D). \tag{8}$$

In which v is the kinematic viscosity of water and our simulation results are listed in Table 2.

Using Einstein relation:

$$D_1 = \lim_{t \rightarrow \infty} \langle |r(t) - r(0)|^2 \rangle / 2t, \tag{9}$$

the diffusion coefficient in the y direction is obtained under different conditions as listed in Table 3.

It is obvious that the diffusion coefficient increases as the dissolubility increase, which has the same change regulation as $v\sqrt{x} / \sqrt{U}$. Previous literature (Sofos et al. 2010) has also considered the liquid diffusion in nanochannels under the effect of the rough walls, and found that the local diffusion coefficient is smaller near a rough wall compared to a smooth wall. In our simulations, as the solute dissolves into the liquid, the solid surface becomes rougher, the results of Sofos et al. further confirm that the fluid-flow is more easily to be Poiseuille-like rather plug-like in a dissoluble channel.

4 Conclusions

Dynamics of dissolutive flow in nanochannels were analyzed using MD simulations. First, the velocity of confined fluid in our simulations was calculated. MKT was used to interpret the velocity profile under different channel widths and dissolubility. Fluid velocity along the cross section presents a plug-like flow in a less dissoluble case like most

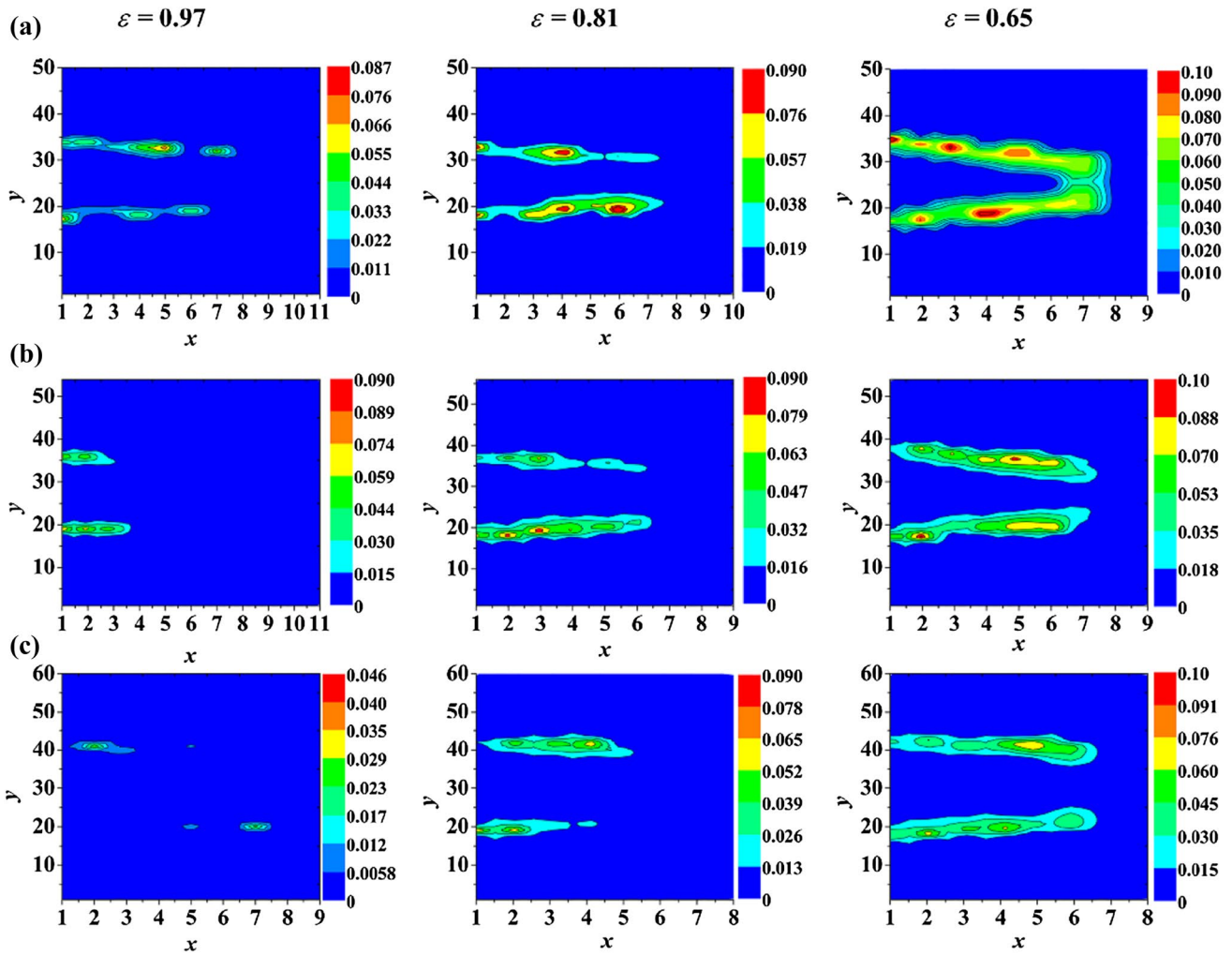


Fig. 7 Concentration distribution of the dissolved particles in nano-channels with different channel widths and dissolubility. **a** $d/D=0.24$, **b** $d/D=0.30$, and **c** $d/D=0.37$. The graphs from left to right shows

the influence of different dissolubility, including, $\epsilon=0.97$, 0.81, and 0.65. (Color figure online)

Table 2 Relation between diffusion and convection $v\sqrt{x}/\sqrt{U}$

	$\epsilon=0.65$	$\epsilon=0.81$	$\epsilon=0.97$
$d/D=0.24$	0.096	0.044	0.039
$d/D=0.30$	0.091	0.047	0.014
$d/D=0.37$	0.095	0.043	0.009

Table 3 Diffusion coefficient D_1 (10^{-9} m²/s) under different conditions

	$\epsilon=0.65$	$\epsilon=0.81$	$\epsilon=0.97$
$d/D=0.24$	0.90	0.46	0.32
$d/D=0.30$	0.89	0.42	0.30
$d/D=0.37$	0.90	0.41	0.31

MD simulations. But with the increase of dissolution, the energy dissipation will gradually change from viscous dissipation to dissolving dissipation, thus a transition from plug-like to Poiseuille-like flow occurs. Besides, the density distribution was analyzed and there exists a critical state depending on the competition between dissolution and size effect. If the dissolution is more important, the liquid density oscillation will disappear due to the disorder of the molecular arrangement and the disruption of the layered structure. But if the size effect dominates, the density is fluctuant as that in inert flow processes. In addition, from the density distribution we obtained a critical state ϵ_c that controls the density transition between fluctuant and uniform state. The number of dissolved particles was also calculated and it satisfies the Boltzmann distribution and ultimately it reaches a stable state. Based on this state,

the scaling relation among the dissolution rate, convection velocity, and diffusion coefficient was obtained when the dissolution capacity is high. Through these investigations, we have recognized that the flow patterns in dissolvable nanochannels can be regulated by changing the dissolubility of solid in liquid and then the dynamics of dissolution behaviors can be controlled and optimized.

This article helps to understand the microscopic mechanisms of dissolutive flow in nanochannels and we hope to provide theoretical support for practical applications.

Acknowledgements This work was jointly supported by the National Natural Science Foundation of China (NSFC, Grant nos. 11722223, 11672300, 11872363 and 51861145314), the CAS Key Research Program of Frontier Sciences (Grant no. QYZDJ-SSW-JSC019), and the Strategic Priority Research Program of the Chinese Academy of Sciences (Grant no. XDB22040401).

References

- Alexiadis A, Kassinos S (2008) The density of water in carbon nanotubes. *Chem Eng Sci* 63:2047–2056
- Amidon GL, Lennernäs H, Shah VP, Crison JR (1995) A theoretical basis for a biopharmaceutical drug classification: the correlation of in vitro drug product dissolution and in vivo bioavailability. *Pharm Res* 12:413–420
- Anderson RY, Kirkland DW (1980) Dissolution of salt deposits by brine density flow. *Geology* 8:66–69
- Bakli C, Chakraborty S (2013) Effect of presence of salt on the dynamics of water in uncharged nanochannels. *J Chem Phys* 138:054504
- Bekri S, Thovert J, Adler P (1995) Dissolution of porous media. *Chem Eng Sci* 50:2765–2791
- Benhassine M, Saiz E, Tomsia AP, De Coninck J (2011) Nonreactive wetting kinetics of binary alloys: a molecular dynamics study. *Acta Mater* 59:1087–1094
- Bentiss F, Lebrini M, Lagrenée M (2005) Thermodynamic characterization of metal dissolution and inhibitor adsorption processes in mild steel/2,5-bis(*n*-thienyl)-1, 3,4-thiadiazoles/hydrochloric acid system. *Corros Sci* 47:2915–2931
- Berendsen H, Grigera J, Straatsma T (1987) The missing term in effective pair potentials. *J Phys Chem US* 91:6269–6271
- Bonn D, Eggers J, Indekeu J, Meunier J, Rolley E (2009) Wetting and spreading. *Rev Mod Phys* 81:739–805
- Brutin D, Starov V (2018) Recent advances in droplet wetting and evaporation. *Chem Soc Rev* 42:558–585
- Chen X et al (2008) Nanoscale fluid transport: size and rate effects. *Nano Lett* 8:2988–2992
- Daccord G (1987) Chemical dissolution of a porous medium by a reactive fluid. *Phys Rev Lett* 58:479–482
- Daccord G, Lenormand R (1987) Fractal patterns from chemical dissolution. *Nature* 325:41–43
- De Gennes P-G (1985) Wetting: statics and dynamics. *Rev Mod Phys* 57:827–863
- Derjaguin B, Obuchov E (1936) Ultramicroscopic analysis of solvate layer and elementary expansion effects. *Acta Phys Chim* 5:1–22
- Dokoumetzidis A, Macheras P (2006) A century of dissolution research: from Noyes and Whitney to the biopharmaceuticals classification system. *Int J Pharm* 321:1–11
- Fan X-J, Phan-Thien N, Yong NT, Diao X (2002) Molecular dynamics simulation of a liquid in a complex nano channel flow. *Phys Fluids* 14:1146–1153
- Granick S (1999) Soft matter in a tight spot. *Phys Today* 52:26–31
- Grujicic M, Cao G, Roy W (2004) Atomistic simulations of the solubilization of single-walled carbon nanotubes in toluene. *J Mater Sci* 39:2315–2325
- Hanasaki I, Nakatani A (2006) Flow structure of water in carbon nanotubes: Poiseuille type or plug-like? *J Chem Phys* 124:144708
- Huang JM, Moore MNJ, Ristorph L (2015) Shape dynamics and scaling laws for a body dissolving in fluid flow. *J Fluid Mech* 765:R3
- Ivanisenko Y, Lojkowski W, Valiev R, Fecht H-J (2003) The mechanism of formation of nanostructure and dissolution of cementite in a pearlitic steel during high pressure torsion. *Acta Mater* 51:5555–5570
- Joseph S, Aluru N (2008) Why are carbon nanotubes fast transporters of water? *Nano Lett* 8:452–458
- Kasiteropoulou K, Karakasidis TE, Liakopoulos A (2013) Mesoscopic simulation of fluid flow in periodically grooved. *Comput Fluids* 74:91–101
- Laidler JK (1941) The theory of rate processes, vol 1. McGraw-Hill, New York, pp 195–196
- Landry K, Eustathopoulos N (1996) Dynamics of wetting in reactive metal/ceramic systems: linear spreading. *Acta Mater* 44:3923–3932
- Lennard-Jones JE (1931) Cohesion. *Proc Phys Soc* 43:461–482
- Liakopoulos A, Sofos F, Karakasidis TE (2017) Darcy–Weisbach friction factor at the nanoscale: from atomistic calculations to continuum models. *Phys Fluids* 29:052003
- Lichter S, Roxin A, Mandre S (2004) Mechanisms for liquid slip at solid surfaces. *Phys Rev Lett* 93:086001
- Martini A, Roxin A, Snurr RQ, Wang Q, Lichter S (2008) Molecular mechanisms of liquid slip. *J Fluid Mech* 600:257–269
- Marzun G, Bönemann H, Lehmann C, Spliethoff B, Weidenthaler C, Barcikowski S (2017) Role of dissolved and molecular oxygen on Cu and PtCu alloy particle structure during laser ablation synthesis in liquids. *ChemPhysChem* 18:1175–1184
- Nagayama G, Cheng P (2004) Effects of interface wettability on micro-scale flow by molecular dynamics simulation. *Int J Heat Mass Transf* 47: 501–513
- Navier CLMH (1823) Mémoire sur les lois mouvement des fluides. *Mem Acad R Sci* 6:389–440
- Netos C, Evans DR, Bonaccorso E, Butt HJ, Craig VS (2005) Boundary slip in Newtonian liquids: a review of experimental studies. *Rep Prog Phys* 68:2859–2897
- Odzak N, Kistler D, Behra R, Sigg L (2014) Dissolution of metal and metal oxide nanoparticles in aqueous media. *Environ Pollut* 191:132–138
- Pismen LM, Rubinstein BY (2001) Kinetic slip condition, van der Waals forces, and dynamic contact angle. *Langmuir* 17:5265–5270
- Plimpton S (1995) Fast parallel algorithms for short-range molecular dynamics. *J Comput Phys* 117:1–19
- Poesio P, Beretta GP, Thorsen T (2009) Dissolution of a liquid microdroplet in a nonideal liquid–liquid mixture far from thermodynamic equilibrium. *Phys Rev Lett* 103:064501
- Ramosalvarado B, Kumar S, Peterson GP (2016) Wettability transparency and the quasiuniversal relationship between hydrodynamic slip and contact angle. *Appl Phys Lett* 108:074105
- Schlichting H, Gersten K (2017) Extensions to the Prandtl boundary–layer theory. *Boundary–layer theory*. Springer, New York, pp 377–411
- Siepmann J, Siepmann F (2013) Mathematical modeling of drug dissolution. *Int J Pharm* 453:12–24
- Singler TJ, Su S, Yin L, Murray BT (2012) Modeling and experiments in dissolutive wetting: a review. *J Mater Sci* 47:8261–8274

- Sofos F, Karakasidis T, Liakopoulos A (2009) Transport properties of liquid argon in krypton nanochannels: anisotropy and non-homogeneity introduced by the solid walls. *Int J Heat Mass Transf* 52:735–743
- Sofos F, Karakasidis TE, Liakopoulos A (2010) Effect of wall roughness on shear viscosity and diffusion in nanochannels. *Int J Heat Mass Transf* 53:3839–3846
- Sofos F, Karakasidis TE, Liakopoulos A (2011) Surface wettability effects on flow in rough wall nanochannels. *Microfluid Nanofluidics* 12:25–31
- Thomas JA, McGaughey AJ (2008) Reassessing fast water transport through carbon nanotubes. *Nano Lett* 8:2788–2793
- Wang F-C, Zhao Y-P (2011) Slip boundary conditions based on molecular kinetic theory: the critical shear stress and the energy dissipation at the liquid–solid interface. *Soft Matter* 7:8628–8634
- Werder T, Walther JH, Jaffe RL, Halicioglu T, Noca F, Koumoutsakos P (2001) Molecular dynamics simulation of contact angles of water droplets in carbon nanotubes. *Nano Lett* 1:697–702
- Yang J, Yuan Q, Zhao Y-P (2018) Evolution of the interfacial shape in dissolutive wetting: coupling of wetting and dissolution. *Int J Heat Mass Transf* 118:201–207
- Yen T-H (2015) Effects of wettability and interfacial nanobubbles on flow through structured nanochannels: an investigation of molecular dynamics. *Mol Phys* 113:3783–3795
- Yin L, Murray BT, Singler TJ (2006) Dissolutive wetting in the Bi–Sn system. *Acta Mater* 54:3561–3574
- Zhou X, De Hosson JTM (1996) Reactive wetting of liquid metals on ceramic substrates. *Acta Mater* 44:421–426

Publisher's Note Springer Nature remains neutral with regard to jurisdictional claims in published maps and institutional affiliations.